Article

Journal of Biomedical Nanotechnology
Vol. 18, 1–12, 2022
www.aspbs.com/jbn

Combined and Single Doxorubicin/Naproxen Drug Loading and Dual-Responsive pH/Ultrasound Release from Flexible Metal-Organic Framework Nanocarriers

Abdollah Karami, Ahmed Ahmed, Rana Sabouni*, Ghaleb A. Husseini, and Vinod Paul

Department of Chemical Engineering, American University of Sharjah, Sharjah, 26666, UAE

In this study, the flexible aluminum-based MIL-53(Al) metal-organic framework was loaded with doxorubicin (DOX) and naproxen (NAP) and was examined as a promising pH/ultrasound dual-responsive drug delivery system. The two drugs were encapsulated in MIL-53(Al) individually to produce the DOX@MIL-53(Al) and NAP@MIL-53(Al) nanocarriers. They were also encapsulated as a dual-drug formulation to produce the DOX* + NAP*@MIL-53(Al) nanocarrier. The MOF nanoparticles were characterized using the Scanning Electron Microscopy (SEM), X-ray diffraction (XRD), Fourier Transform Infrared spectroscopy (FTIR), and Dynamic Light Scattering (DLS) techniques. In the case of the DOX@MIL, the nanocarriers' drug Encapsulation Efficiency (EE) and Encapsulation Capacity (EC) were 92% and 16 wt.%, respectively, whereas, in the case of NAP@MIL-53(Al), the average NAP EE and EC were around 97.7% and 8.5 wt.%, respectively. On the other hand, in the DOX* + NAP*@MIL-53(Al) nanoparticles, the average DOX* EE and EC were 38.9% and 6.22 wt.%, respectively, while for NAP*, the average EE and EC were 70.2% and 4.49 wt.%, respectively. *In vitro* release experiments demonstrated the good pH and Ultrasound (US) dual-responsiveness of these nanocarriers, with a maximum US-triggered DOX and NAP release, at a pH level of 7.4, of approximately 53% and 95%, respectively. In comparison, the measured release was around 90% and 36% at pH 5.3 for DOX and NAP, respectively. In the case of the dual-drug formulation, the nanocarrier displayed similar pH/US dual-responsive behavior. Finally, the 3-(4,5-dimethylthiazol-2-yl)-2,5-diphenyltetrazolium bromide (MTT) results confirmed the biocompatibility and low cytotoxicity of MIL-53(Al) at concentrations up to 1000 μg/ml.

KEYWORDS: *Metal-Organic Frameworks (MOFs), Drug Delivery, Drug Codelivery, Ultrasound, Triggered Release, Stimuli-Responsive Nanocarriers, Doxorubicin, Naproxen, MIL-53(Al).*

INTRODUCTION

Cancer has impacted the majority of the world's population, and it remains one of the major causes of death worldwide [1]. One of the major treatment methods employed against malignancies is chemotherapy; however, this mode of therapy is plagued with severe side effects, such as nausea, fatigue, infections, hair loss, irritation at the site of injection, in addition to cardiac and gastrointestinal problems [2] that severely compromise the quality of life of cancer patients. Consequently, nanoparticles such as liposomes, polymeric micelles, and mesoporous silica have been examined as potential anticancer drug nanocarriers. Such nanocarriers can encapsulate the anticancer drug, allowing for the targeted drug delivery at the tumor site, hence reducing the side effects of chemotherapy and increasing the bioavailability of the drug and the overall treatment efficacy [3–5].

Due to their favorable characteristics, metal-organic frameworks (MOFs) gained massive interest in various biomedical applications, one of which is drug delivery [6–11]. Metal-organic frameworks have outstanding physical and chemical properties, including high porosity, pore size tunability, high surface area, and excellent biocompatibility [12–15]. These characteristics allow MOFs to be utilized as efficient drug delivery carriers by encapsulating therapeutic agents utilizing absorption or adsorption mechanisms. In addition, MOFs enhance the bioavailability and efficiency of the treatment by providing slow drug release, controlled by various mechanisms, including

*Author to whom correspondence should be addressed.
Email: rsabouni@aus.edu
Received: 25 May 2022
Accepted: 6 July 2022

matrix degradation, and providing active and passive targeting functionalities [16].

The first generation of MOF drug nanocarriers was developed by encapsulating drug molecules into the nanovehicles pores through adsorption. These nanocarriers provided drug release with minimal to no stimulus by particles disintegrating into the tumor microenvironment (TME) [11]. In recent years, the field of MOF-based nanocarriers exhibited appealing progress with the development of stimuli-responsive MOF-based nanoparticles as drug delivery systems (DDSs). The versatility of MOFs in terms of chemical modification and/or size control has allowed the possibility of designing stimuli-responsive MOF-based DDSs with enhanced drug loading and controlled drug release kinetics, while maintaining chemical/colloidal stability under physiological conditions [17]. These MOF-based DDSs utilize single or multi stimuli that can be classified as endogenous or exogenous [10, 11, 18, 19]. Endogenous stimuli are usually dependent on chemical and/or biological triggers such as pH changes, ions, redox agents, ATP, enzymes, DNAzymes, miRNAs, or aptamer–ligand complexes. On the hand, exogeneous stimuli, including light, heat, magnetic field, microwave irradiation and ultrasound, are typically independent of the physiological conditions inside the body. The main advantage of exogenous stimuli over their endogenous counterparts is that they allow a better spatiotemporal/dosage control of drug release [20]. In other words, the drug release can be triggered or stopped by activating and deactivating the stimulus. However, it can be challenging for external stimuli to penetrate the body to reach the tumor site, thus limiting the efficacy of this type of drug delivery.

Recently, multi stimuli-responsive MOF nanocarriers that combine two or more internal/external triggers have been developed. For instance, dual-responsive MOF-based nanocarrier is an example of DDSs that utilize combined pH and ultrasound (US) stimuli [21–23]. The application of noninvasive low-frequency US improves drug delivery by enhancing the nanocarrier's diffusion into the cancerous cells and increasing the targeted payload release due to the thermal effects and mechanical stresses generated by the acoustic waves [24–27].

In this work, an aluminum-based metal-organic framework, MIL-53(Al), is investigated as a promising stimuli-responsive (pH and US) MOF-based DDS for the delivery and codelivery of doxorubicin hydrochloride (DOX) and naproxen sodium (NAP). The MOF consists of aluminum (Al) metal nodes coordinated to benzene-1,4-dicarboxylate (BDC) organic linkers. MIL-53(Al) is a well-known MOF that has demonstrated remarkable results in various environmental applications [28–35] due to its flexibility and water stability [36]. Many studies have reported using MOF-based nanocarriers with excellent drug loading and release efficiencies [20]. However, most of these studies have focused on encapsulating one drug into the MOF nanoparticles, which has drawbacks in cancer chemotherapy due to multidrug resistance (MDR) [37]. As a result, it is desired to design a nanocarrier that offers high loading and release efficiencies for the codelivery of multiple drugs to overcome the MDR effect. Another benefit of a codelivery DDS is the possibility of encapsulating a therapeutic drug that mitigates the severe complications associated with conventional chemotherapy. In this study, DOX and NAP were selected as model drugs. DOX is a chemotherapeutic drug commonly used to treat various cancers such as breast, lung, ovarian, non-Hodgkin's, and Hodgkin's lymphoma [38]. At the same time, NAP (commercial name Aleve) is a non-steroidal anti-inflammatory drug (NSAID) that is commonly prescribed for pain, fever, and inflammation [39]. Furthermore, NSAIDs have been reported to have cancer inhibitory effects. *In vivo* and *in vitro* studies have found that combining chemotherapy with NSAIDs enhances treatment efficacy and may circumvent the MDR effect [40–45]. Therefore, a combined-drug nanocarrier can be a promising DDS to realize efficient cancer treatment.

Herein, we report the encapsulation of DOX and NAP in the pores of MIL-53(Al) as single and dual-drug formulations. To the best of our knowledge, this manuscript is the first study to report the combined pH/US-triggered codelivery of DOX and NAP using MOF-based noncarriers. The produced nanoparticles were characterized using scanning electron microscopy (SEM), X-ray diffraction (XRD), Fourier-transform infrared (FTIR) spectroscopy, and dynamic light scattering (DLS). In addition, to demonstrate the pH/US dual-responsive capability of this novel DDS, the *in vitro* drug release profiles of DOX and NAP from MIL-53(Al) were measured in phosphate-buffered saline (PBS) at two pH levels (7.4 and 5.3) and 37 °C, with and without low-frequency ultrasound (LFUS, 35 kHz). Finally, the cytotoxicity of MIL-53(Al) was tested on MCF-7 breast cancer cells via the MTT assay.

EXPERIMENTAL DETAILS

Materials

The MOF nanocarriers, MIL-53(Al), were obtained as Basolite® A100 from Sigma–Aldrich (supplied through LABCO LLC. Dubai, United Arab Emirates). Phosphate-buffered saline (PBS) tablets were also obtained from Sigma-Aldrich to prepare 0.1 M PBS. Aqueous HCl or NaOH solutions (1 M) were used for the pH adjustment of the PBS solution. The chemotherapeutic drug doxorubicin hydrochloride (DOX) was obtained from Euroasia Trans Continental (Mumbai, India), while Naproxen sodium (NAP) was purchased from Sigma–Aldrich (supplied through LABCO LLC. Dubai, United Arab Emirates).

Characterization

The MIL-53(Al) morphology was examined using field emission scanning electron microscopy (FE-SEM). The X-ray diffraction (XRD) patterns of the nanocarriers were collected using a Bruker D8 Advance X-ray diffractometer (Billerica, Massachusetts, USA) at room temperature using a Cu K_α radiation source ($\lambda = 1.54$ Å) on a silicon wafer from 5.0 to 60° (2θ) with a step size of 0.03° and 1 s (per step) in a continuous mode. The FTIR spectra were measured using an FTIR instrument (PerkinElmer, Waltham, Massachusetts, USA), operating in the range of 4000 to 450 cm^{-1}, with a step of 1.0 cm^{-1}. The average particle diameter and polydispersity index (PDI) of the MIL-53(Al) nanoparticles were determined using a dynamic light scattering instrument (DynaPro NanoStar, Wyatt Technology, Santa Barbara, CA, USA). The UV-Vis spectra of the MOF samples were collected using a UV-Visible Spectrophotometer (UV-2600, Shimadzu, Japan) equipped with Diffuse Reflectance Spectroscopy (DRS). The thermal stability of the MIL-53(Al) was investigated using the Mettler Toledo Thermal gravimetric Analysis 851e model (Mississauga, ON, Canada). The samples were heated from 25 °C to 800 °C at a heating rate of 10 °C/min under nitrogen purge (50 mL/min).

Single and Combined DOX/NAP Calibration Curve

In order to quantify the amount of DOX and NAP released from the MIL-53(Al) nanocarriers, standard single/dual DOX and NAP solutions in PBS at two pH levels (4.7 and 5.3) were prepared. In the single drug solutions, the DOX concentration range was 0.0156–0.25 mM, while the NAP concentration range was 0.004–0.032 mM. on the other hand, the DOX and NAP concentration range in the combined drug solutions was 0.01–0.05 and 0.004–0.032 mM, respectively. Then, the absorbance of the prepared solutions was measured using an Evolution™ 60S UV-Vis spectrophotometer (Thermo Scientific, Waltham, MA, USA) between 190–600 nm, and the calibration curve was generated by determining the DOX and NAP absorbance at their respective characteristic peak (480 and 320 nm, respectively).

Single and Combined DOX/NAP Encapsulation and *In Vitro* Release

DOX and NAP were encapsulated in MIL-53(Al) nanoparticles as single and combined drugs. Figure 1 presents a schematic illustration of the single and dual-drug encapsulation into MIL-53(Al). DOX and NAP were dissolved in deionized water (DI) to obtain 1 mM DOX and NAP solutions for the single drug formulation. Both DOX and NAP were dissolved in DI in equimolar ratios for the dual drug encapsulation experiments. The encapsulation procedure was performed by adding 15 mg of MIL-53(Al) nanoparticles to a 5 ml drug solution and stirring in the dark,

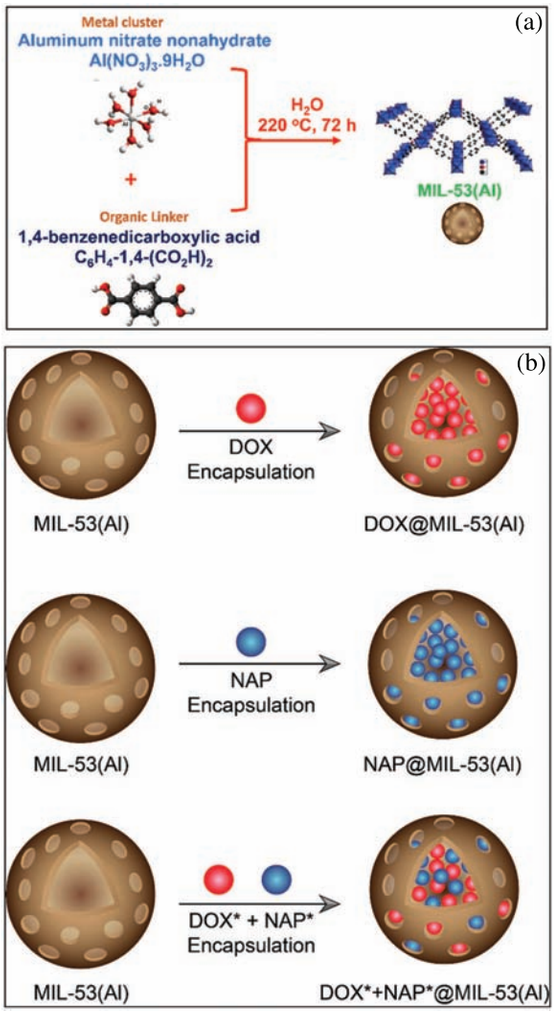

Figure 1. A schematic illustration of (a) MIL-54 synthesis and, (b) DOX and NAP encapsulation into MIL-53(Al) nanoparticles.

to avoid DOX degradation as Dox is light sensitive, at room temperature for 24 hours. The mixture was then centrifuged at 4500 rpm for 30 minutes (Heraeus Megafuge 8R, Thermo Scientific, Waltham, MA, USA). Next, the supernatant was removed and analyzed using UV-Vis spectroscopy at the respective characteristic peak of DOX and NAP. The DOX@MIL-53(Al), NAP@MIL-53(Al), and DOX* + NAP*@MIL-53(Al) nanoparticles were then washed twice and centrifuged.

The drug encapsulation efficiency (EE) was calculated using Eq. (1).

$$\text{EE}\ (\%) = \frac{C_i - C_f}{C_i} \times 100 \qquad (1)$$

where C_i and C_f are the initial and final drug concentrations in the supernatant solution, respectively.

Additionally, the encapsulation capacity (EC) of the drug is calculated using the following equation:

$$\text{EC (wt.\%)} = \frac{m_{\text{drug}}}{m_{\text{drug}} + m_{\text{MOF}}} \times 100 \quad (2)$$

where m_{drug} is the mass of encapsulated drug (mg) and m_{MOF} is the mass of the MIL-53(Al) before loading (mg).

The *in vitro* release experiments were conducted for the DOX@MIL-53(Al), NAP@MIL-53(Al), and DOX* + NAP*@MIL-53(Al) nanoparticles at two pH levels, 7.4 and 5.3, where the neutral pH represents the physiological conditions of the body and the 5.3 pH simulates the acidity of the endosome in tumor cells [46, 47]. Also, the release experiments were conducted with and without the application of low-frequency ultrasound (LFUS, 35 kHz). In each case, 15 mg of the nanoparticles was added to a 5 ml PBS solution at 7.4 and 5.3 pH levels and a temperature of 37 °C. The US-triggered release was also investigated at the two pH levels. In each case, *in vitro* release experiments were conducted in a sonication bath (SHE-UT8031-EUK, Shesto, Watford, UK) at a frequency of 35 kHz. The US was applied in a 15 min cycle. After each sonication cycle, the samples were centrifuged, and an aliquot (~3 ml) was taken from the supernatant for UV-Vis spectroscopic analysis. The exact amount of the aliquot was replaced with fresh PBS for the next release cycle. Control *in vitro* release experiments were also conducted in the absence of ultrasound. All experiments were performed in triplicates, and the average release profiles were reported ± the standard deviation. The cumulative release percentage (CR%) was calculated using Eq. (3):

$$\text{Cumulative release percentage (CR\%)} = \sum_i \left(\frac{N_i}{N_m} \right) \quad (3)$$

where N_i is the amount of the drug (mmol) in the aliquot at each time point and N_m is the maximum drug release possible (mmol), determined via the spectroscopic analysis of the supernatant collected after the loading step.

In Vitro Cytotoxicity Analysis by MTT Assay

The MCF-7 breast cancer cell line was purchased from The European Collection of Authenticated Cell Cultures (ECACC). RPMI-1640, Trypsin EDTA, and Fetal Bovine Serum (FBS) were purchased from PAN-Biotech (Aidenbach, Germany). MCF-7 cells were cultured in RMPI-1640 supplemented with 10% FBS at 37 °C and 5% CO_2. Cells growing in culture flasks, in the exponential phase of growth, were trypsinized, collected, and seeded into 24-well plates at a concentration of 50000 cells per well. After 24 hours of incubation at 37 °C and 5% CO_2, the culture media was changed with fresh media containing the MIL-53(Al) at different concentrations (31.25 to 1000 μg/ml), non-treated wells were kept as control. The well plates were then incubated for another 48 hours to study the cytotoxic effect of the MIL-53(Al) particles. After 48 hours of treatment, MTT was added to each well at a concentration of 0.5 mg/ml, followed by another 4-hours incubation to allow the formation of purple color formazan crystals. Once the incubation was completed, the media in the wells were discarded, and 250 μl of DMSO was added to dissolve the formazan crystals. The intensity of the purple color (which is proportional to the cell viability) was measured using a plate reader (Metertech M965, Taipei, Taiwan) at 600 nm. The cell viability was calculated as follows:

$$\%\ \text{Cell Viability} = \frac{\text{The average absorbance value of the treatment group}}{\text{The average absorbance value of the control}} \times 100 \quad (4)$$

MTT assays run with Dox were performed as shown above. However, after overnight incubation at 37 °C and 5% CO_2, the cells were treated with DOX-loaded MOF at concentrations of 50 and 100 μg/ml. After the cells were treated, one well plate was kept as a control in the incubator. The other plate was kept in a water bath and subjected to ultrasound at 20 kHz using a sonicating probe placed adjacent to the well-plate for 4 minutes.

RESULTS AND DISCUSSION

Characterization

The shape and surface morphology of MIL-53(Al) nanoparticles were characterized by SEM and are shown in Figure 2. The results show the well-crystallized needle-like nanosized particles, which are similar to previously reported ones [48, 49]. Further SEM imaging proved that the morphology of MIL-53(Al) after being loaded with combined DOX and NAP is not altered (Fig. 2(b)), indicating the structural stability of the MIL-53(Al) particles after encapsulation. The presence of larger particles is attributed to the uneven distribution and agglomeration of particles while preparing the particles for the SEM grid.

Figure 3 presents the XRD patterns of the MIL-53(Al), DOX@MIL-53(Al), and NAP@MIL-53(Al) nanoparticles. The main characteristics of diffraction peaks at 8.9°, 15.2°, 17.86° correspond to the peak position reported in the literature [50, 51]. Furthermore, these peaks confirm the crystallinity of the nanoparticles, which is similar to previously reported patterns [48–50, 52]. Furthermore, the XRD results of the drug-loaded MOFs, DOX@MIL-53(Al) and NAP@MIL-53(Al) confirm the successful encapsulation of drug molecules within the framework of the nanocarrier, as demonstrated by the broadening and weakening of the detected peaks [53]. Although MIL-53(Al) after encapsulation possessed a broader peak, yet it sustained its crystalline structure indicating the stability of the MIL-53(Al) nanoparticles. This phenomenon has been reported previously (referred to as the breathing effect). It is attributed to

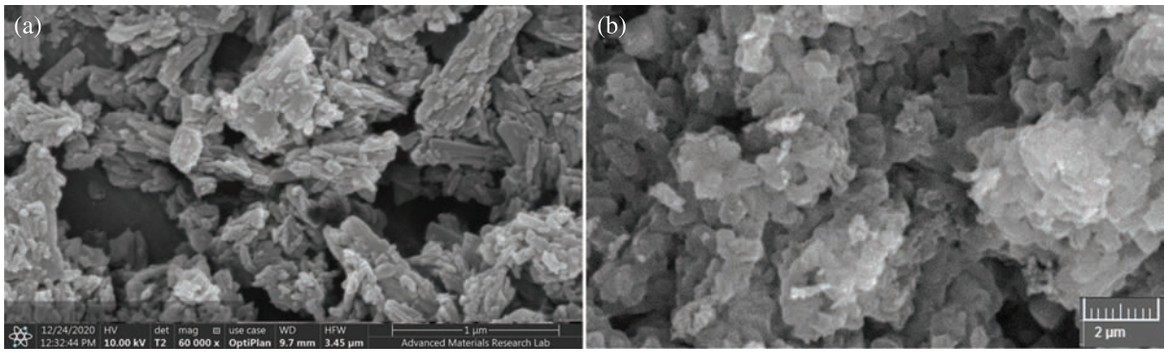

Figure 2. **SEM images of (a) MIL-53 and, (b) drug-loaded MIL-53(Al) nanoparticles.**

the MIL-53(Al) framework's flexibility as its pores expand when the adsorbed drug molecules diffuse into the MOF's pores [54].

The FTIR analysis presented in Figure 4 shows the changes in the MIL-53(Al) absorption peaks due to DOX and NAP encapsulation into the nanoparticles. The measured IR spectrum of MIL-53(Al) is similar to previously reported results in the literature [50, 55]. The absorption peaks at 1690 and 1596 cm^{-1} correspond to the COO– asymmetric bond stretching vibration, while the peaks at 1510 and 1416 cm^{-1} may be attributed to the corresponding symmetric stretching vibration [48]. The absorption peak at around 3424 cm^{-1} corresponds to the –OH stretching vibration [55]. The FTIR spectra of the DOX/NAP-loaded MIL-53(Al) showed a slight increase in the intensities and widening of the absorption peaks, which may signal the interaction between the encapsulated drug molecules and the nanocarrier.

The average particle size was determined via the dynamic light scattering technique (DLS). The particle size distribution is shown in Figure 5. The results showed that the average hydrodynamic particle diameter of MIL-53(Al) was around 477 nm, with around 83% of the particles having around 382.2 nm particle diameter. Furthermore, the polydispersity index (PDI) was determined to be 0.312. DOX and NAP@MIL-53(Al) DLS results were in good comparability with MIL-53(Al) before encapsulation,

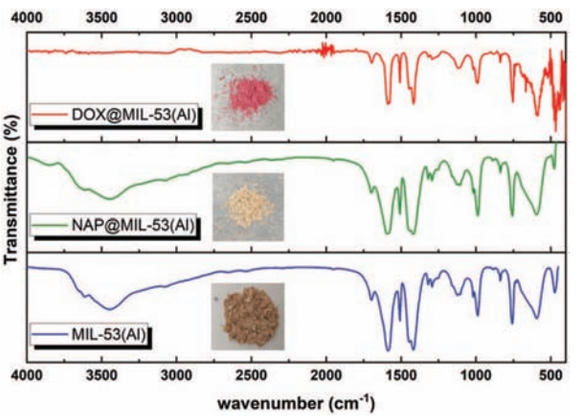

Figure 4. **FTIR spectra of MIL-53(Al), DOX@ MIL-53(Al), and NAP@ MIL-53(Al) nanoparticles. The insets represent the pictures of the MIL-53(Al) and drug-loaded MIL-53(Al) nanoparticles.**

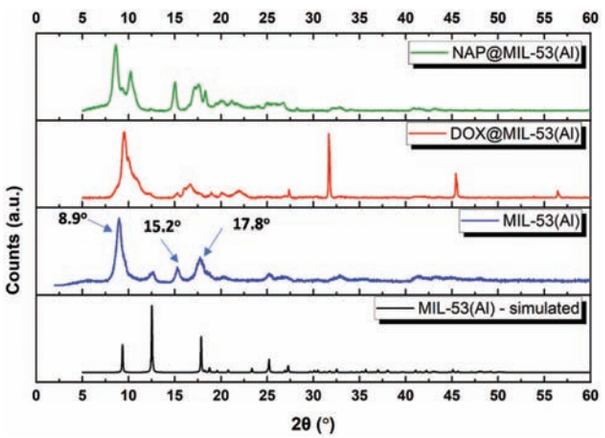

Figure 3. **XRD patterns of MIL-53(Al), DOX@ MIL-53(Al), and NAP@ MIL-53(Al) nanoparticles. The simulated pattern was obtained from the Cambridge Crystallographic database.**

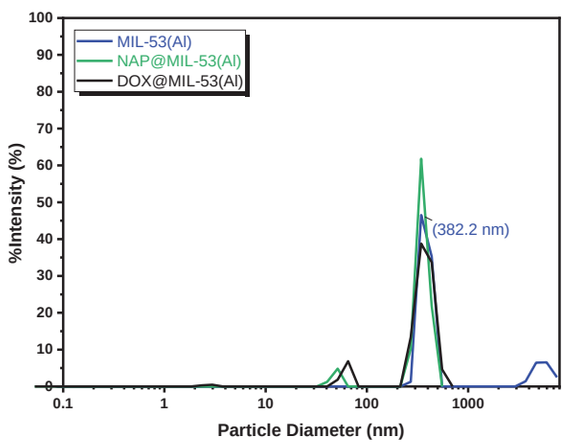

Figure 5. **Particle size distribution of MIL-53(Al), DOX@ MIL-53(Al), and NAP@ MIL-53(Al) nanoparticles.**

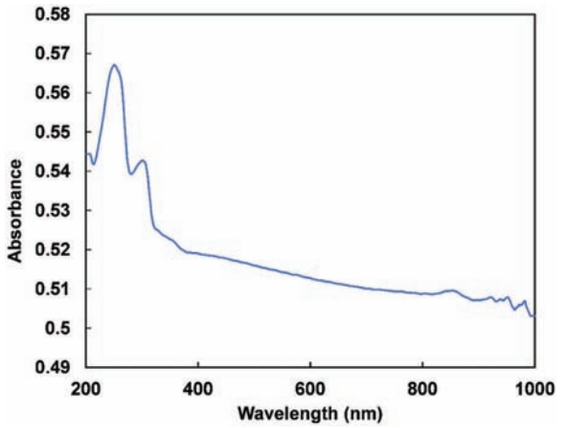

Figure 6. **UV-Vis spectra of MIL-53(Al).**

indicating good polydispersity [56]. The DLS results show that the average particle size of the nanocarrier is suitable for drug delivery applications as the vascular pore cutoff size can reach up to μm sizes [57–61]; depending on the targeted organ, the size of the fenestrations of the vasculature in that organ, type and location of the tumor, and the route of nanocarrier's administration (intravenous injection, tumor injection, oral, etc.) [57, 60–62].

The UV-Vis spectra of MIL-53(Al) shown in Figure 6, exhibits a maximum characteristic peak at 256 and almost no absorbance in the visible region, which is in good agreement with the literature [63].

The TGA analysis shown in Figure 7 reveals the thermal stability of the MIL-53(Al) up to 400 °C. Beyond that, the MOF starts to decompose. Two distinguished weight losses can be observed. The initial weight loss below 100 °C could be attributed to the dehydration process due to the evaporation of water molecules trapped within the pores of MIL-53. While the second major weight reduction was observed at ∼400 °C, corresponding to the decomposition

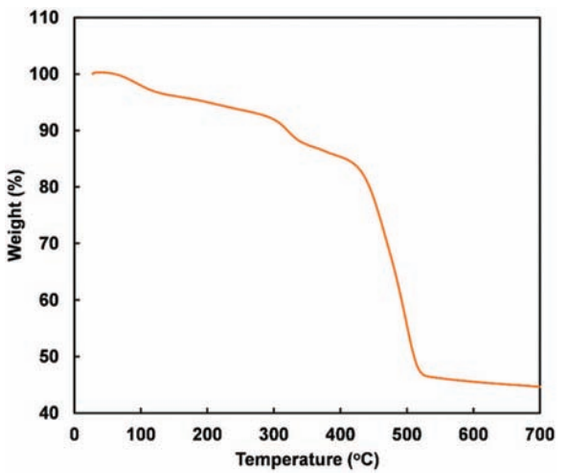

Figure 7. **Thermal gravimetric analysis (TGA) of MIL-53(Al).**

of the terephthalic acid ligand in the organic framework [64, 65].

Single and Combined DOX/NAP Encapsulation and *in Vitro* Release

In this work, DOX and NAP are loaded into MIL-53(Al) as an individual (single) and combined formulations. Then, the encapsulation efficiency (EE) and capacity (EC), and the *in vitro* release for each formulation are assessed. First, the single drug EE and EC of MIL-53(Al) nanoparticles were determined by measuring the UV-Vis absorbance spectra of the DOX/NAP initial solutions and the final supernatant after separation by centrifugation. Then Eqs. (1) and (2) were used to calculate the EE and EC. Figure 8 shows the UV-Vis absorbance spectra of the DOX and NAP standard solutions and the calibration curves used to calculate the drug concentration in PBS. The experimental results (triplicates) showed that the average DOX EE and EC in MIL-53(Al) were around $92 \pm 2.2\%$ and 16 ± 0.05 wt.%, respectively, whereas the average NAP EE and EC were around $97.7 \pm 0.05\%$ and 8.5 ± 0.04 wt.%, respectively. In general, the high encapsulation efficiency for DOX and NAP can be related to the strong drug/MIL-53(Al) interaction which contributes to the effective adsorption of the drug's molecules inside the pores of the nanocarrier. In the case of DOX@MIL-53(Al), these interactions are usually attributed to hydrogen bonding, π–π stacking, and coordination with the free uncoordinated metal sites in the framework [66–68]. Similarly, in the case of NAP@MIL-53(Al), the drug/nanocarrier interactions are usually due to the formation of hydrogen bonding as well as π–π stacking [34, 69].

The UV-Vis absorbance spectra of the combined DOX* and NAP* standard solutions are presented in Figure 9. The asterisk symbol (*) indicates that the drugs are loaded in combination into the nanocarrier's matrix. Similar to the single drug solutions, the calibration curves were used to calculate the concentration of DOX and NAP in the drug solutions. Experimental results showed that for both DOX* and NAP*, the EE and EC were lower than in the case of single DOX and NAP; For DOX*, the average EE and EC were $38.9 \pm 0.80\%$ and 6.22 ± 0.13 wt.%, respectively, while for NAP*, the average EE and EC were $70.2 \pm 8.22\%$ and 4.49 ± 0.54 wt.%, respectively. The drop in the encapsulation efficiency and capacity for both drugs is expected due to the competition between DOX* and NAP* molecules diffusing into the matrix of MIL-53(Al). The higher NAP* EE relative to DOX* can be attributed to the relatively smaller molecular weight of NAP compared to DOX, which may contribute to NAP* molecules diffusing relatively better than the DOX* molecules into the nanocarrier's framework.

The pH/US-triggered release profiles of DOX and NAP from MIL-53(Al) are presented in Figure 10. The experiments were conducted *in vitro* at two pH conditions

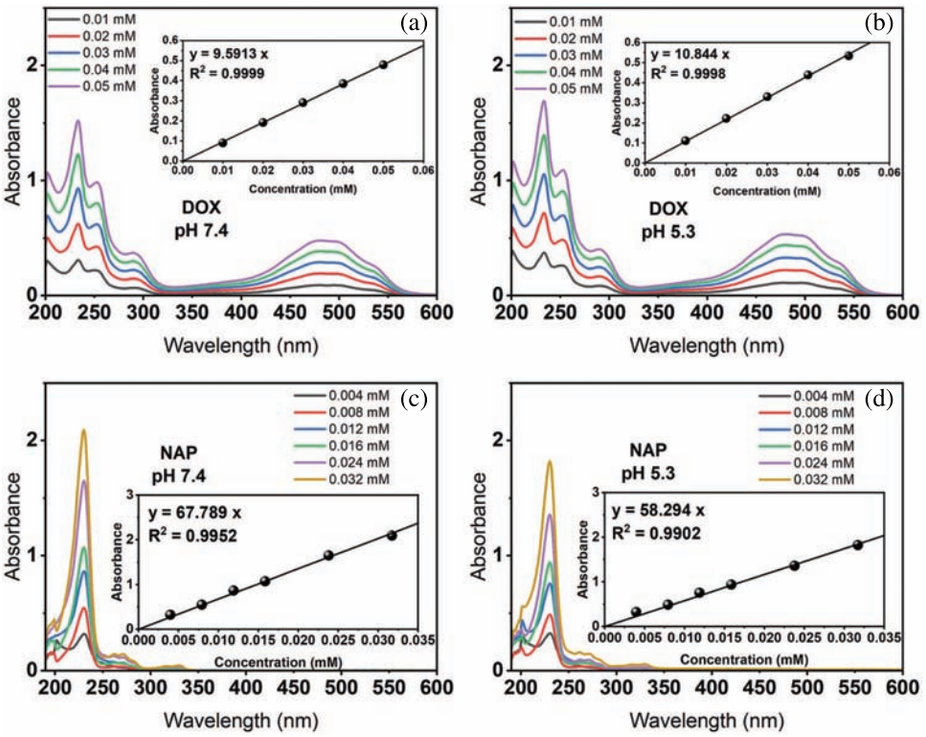

Figure 8. **UV-Vis absorbance spectra of the standard single drug solutions. (a–b) DOX in PBS (pH 5.3 and 7.4) and (c–d) NAP in PBS (pH 5.3 and 7.4). Insets represent the calibration curves.**

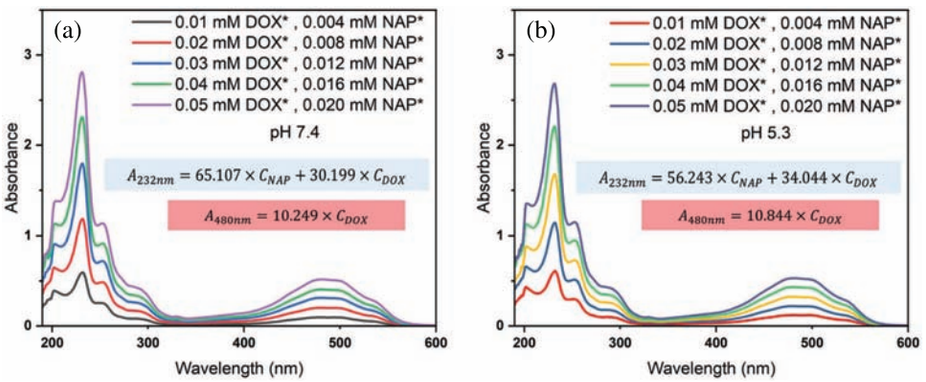

Figure 9. **UV-Vis absorbance spectra of the standard combined DOX* + NAP* solutions. The insert equations represent the absorbance equations at 232 and 480 nm as functions of the NAP* and DOX* concentrations in the combined drug formulation. Based on the measured spectra of the samples, DOX* concentration was calculated using the absorbance at 480 nm (equation highlighted in red). Then, the calculated value was used to calculate NAP* concentration from the absorbance equation at 232 nm (equation highlighted in blue).**

(7.4 and 5.3), including a control group to study the significance of US as a triggering stimulus. The release profiles were produced using the average of three experimental replicas, with error bars representing the standard deviation. The results demonstrate the nanocarrier's dual-responsive capability (pH and US). In the case of DOX@MIL-53(Al), the application of US as a stimulus increased the cumulative release percentage (CR%) of DOX from around $11 \pm 1.06\%$ to $53 \pm 1.66\%$ and from $28 \pm 4.06\%$ to $90 \pm 0.42\%$ at pH levels 7.4 and 5.3, respectively (Figs. 10(a and b)). The enhanced DOX release due to the application of US can be attributed to the oscillatory formation of acoustic cavities, which leads to mechanical stresses destabilizing the nanoparticles' structure, and causing the enhanced release of the loaded drug [26]. Furthermore, the higher DOX CR% at pH 5.3 could be attributed to the protonation of the amnio group of the DOX. Hence, it is revealed that the pH-sensitive

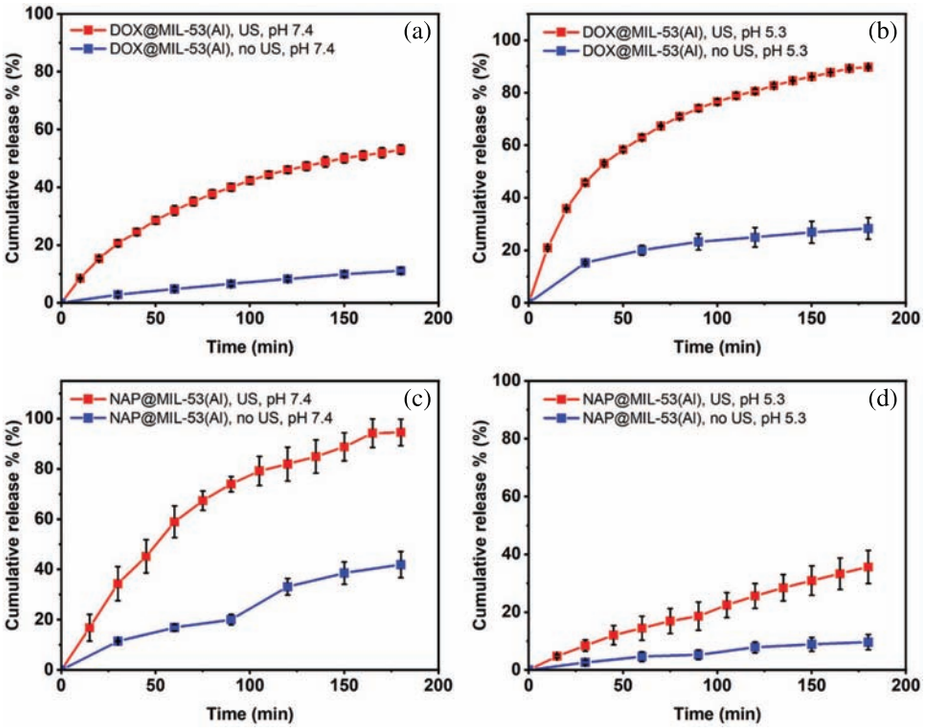

Figure 10. ***In vitro*** **release profiles of DOX and NAP. The error bars represent the standard deviation of the three replicates, while the points represent the average of these three independent replicates.**

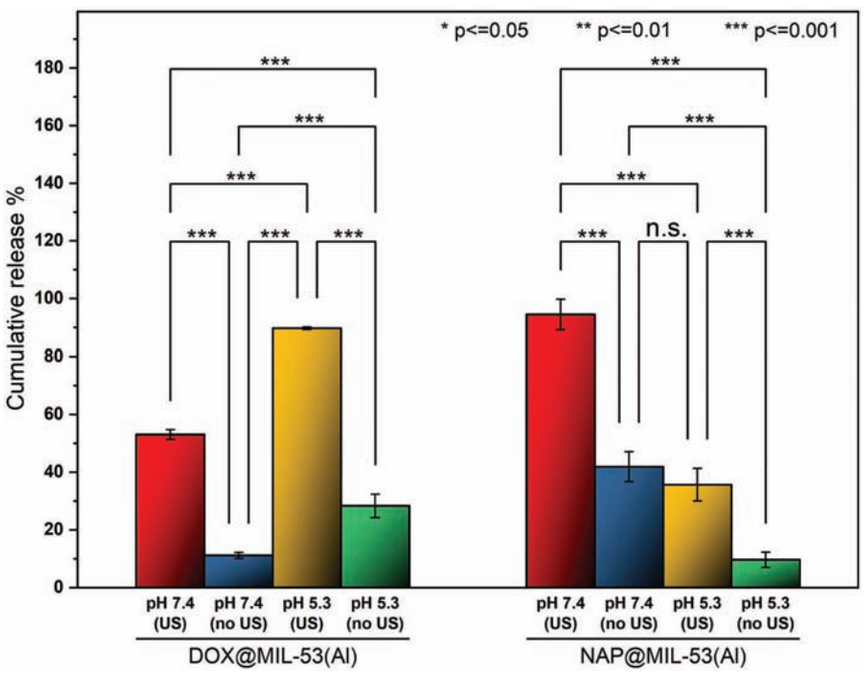

Figure 11. **Combined** ***in vitro*** **DOX and NAP cumulative release percentage at two pH levels (7.4 and 5.3) and 37 °C. (*n* = 3, error bars represent the standard deviation, and p-values were determined using ANOVA with Tukey's method).**

behavior of MIL-53(Al) could effectively release DOX in acidic environment while reducing its leakage during long blood circulations at higher pH. In particular, this selective release of MIL-53(Al) nanoparticles, embraces it as desirable feature in anticancer drug delivery systems (DDSs), as the cancer tissues or the tumor microenvironment (TME) is more acidic compared to the health tissues [21]. Similar to the DOX-loaded nanoparticles, the application of US stimulus increased NAP CR% from NAP@MIL-53(Al) nanoparticles from around $42 \pm 5.22\%$ to $95 \pm 5.29\%$ and from $10 \pm 2.61\%$ to $36 \pm 5.69\%$ at pH 7.4 and 5.3, respectively (Figs. 10(c and d)). However, these results revealed the opposite pH-responsive behavior of the NAP@MIL-53(Al) nanoparticles compared to the DOX@MIL-53(Al) nanoparticles, as the NAP CR% was higher at the higher pH level (7.4).

The *in vitro* release data for DOX and NAP were analyzed for statistical significance using the analysis of variance (ANOVA) test combined with Tukey's method. The statistical significance level was set at a 95% confidence interval ($P < 0.05$). The ANOVA results presented in Figure 11 show that US-triggered DOX and NAP release from DOX@MIL-53(Al) and NAP@MIL-53(Al), respectively, at both pH levels (7.4 and 5.3) were statistically significant ($P \leq 0.001$). Furthermore, the effect of pH on the release of DOX and NAP was found to be statistically significant with and without the application of US ($P \leq 0.001$).

Figure 12 displays the *in vitro* cumulative release profiles of DOX* and NAP* from DOX* + NAP*@MIL-53(Al) nanocarriers. The results revealed that the pH/US-triggered CR% of the combined drug formulation was significantly slower than in the formulation of the individual drug within the same period (3 hours), which was characterized by initial fast kinetics within the first hour, followed by slowing release as time progresses. At the neutral pH (7.4), the maximum US-triggered release of DOX* and NAP* from DOX* + NAP*@MIL-53(Al) was around $0.2 \pm 0.02\%$ and $3 \pm 0.47\%$, respectively, while at pH 5.3, the maximum US-triggered *%CR* was around $0.3 \pm 0.02\%$ and $1.5 \pm 0.21\%$ for DOX* and NAP*, respectively. Hence, the effect of pH/US on the release of DOX* and NAP* was similar to that observed in the case of DOX and NAP release. Furthermore, the slow release kinetics of DOX* relative to NAP* under the same release conditions may be due to the formation of coordination bonds between the free metal sites and the DOX* molecules [67, 68]. These results reveal that the combined drug formulation of DOX* + NAP*@MIL-53(Al) is a promising nanocarrier, as it can be used as an implantable drug delivery system (DDS) that can offer prolonged drug release; hence, higher drug bioavailability and reduced complications stemming from chemotherapy-related side-effects.

In-Vitro Cytotoxicity Analysis by MTT Assay

The cytotoxicity analysis of the nanoparticles was investigated by treating the MCF-7 breast cancer cell lines

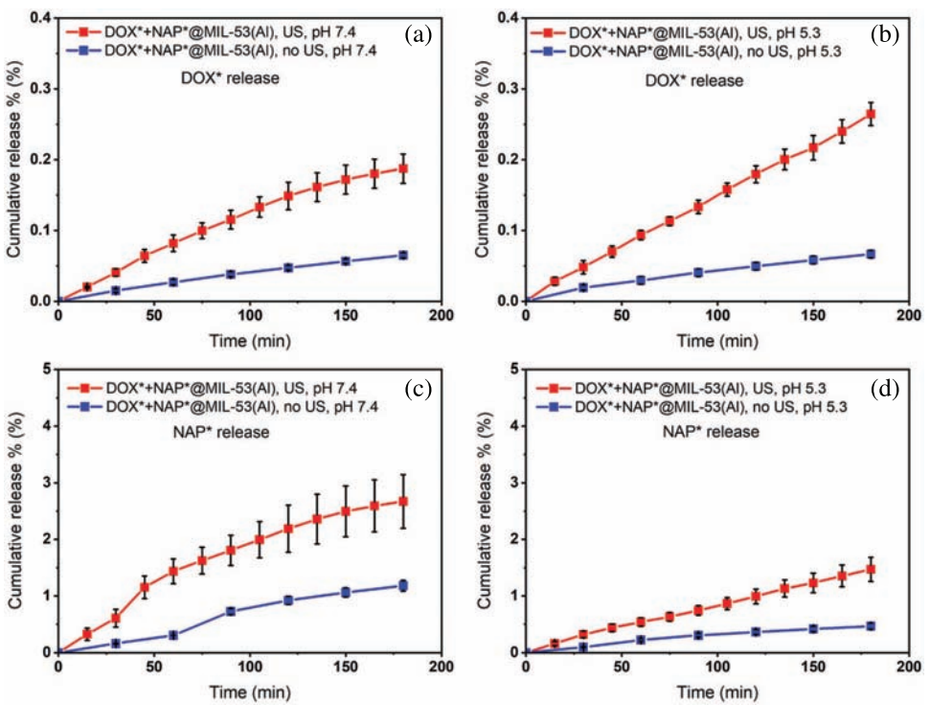

Figure 12. ***In vitro*** **release profiles for combined DOX* and NAP*. The error bars represent the standard deviation of the three replicates, while the points represent the average of these three independent replicates.**

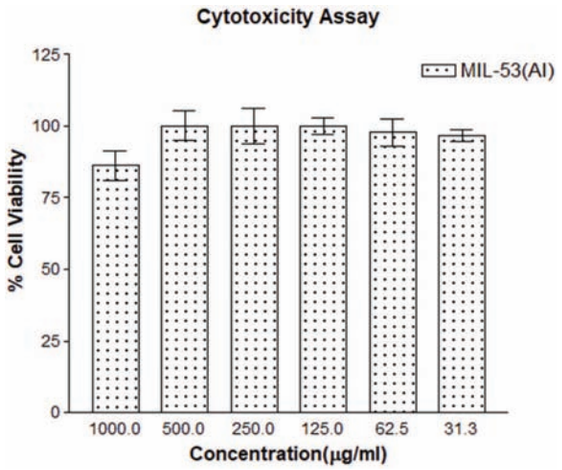

Figure 13. Cytotoxicity analysis of MIL-53(Al) via MTT assay at different concentrations.

with the nanoparticles at different concentrations (ranging between 31.25 and 1000 μg/ml). The results are presented in Figure 13. Even after the 48-hour treatment at the higher concentration of 1000 μg/ml, the MIL-53(Al) was not very toxic (the average cell viability was above 80%), signifying the biocompatibility of the nanoparticle. Additionally, the MTT assay performed with Dox-encapsulated MOFs showed statistical significance in viabilities between sonicated and incubated cells. After the cells were treated with DOX-loaded MOF at concentrations of 50 and 100 μg/ml, one well plate was kept as a control in the incubator. The other plate was kept in a water bath and subjected to 20-kHz ultrasound using a sonicating probe placed adjacent to the well-plate for 4 minutes. The cell viabilities of incubated and sonicated cells at a concentration of 50 μg/ml were $44.2\% \pm 1.4\%$ and $39.5\% \pm 1.6\%$, respectively (P-value $= 0.002077$). While at 100 μg/ml, experiments showed viabilities of $26.2\% \pm 2.2\%$ (incubated) versus $18.3\% \pm 2.5\%$ (sonication), with a p-value of 0.001575.

CONCLUSIONS

In this work, flexible MIL-53(Al) nanoparticles were successfully loaded with the anticancer drug DOX and the non-steroidal anti-inflammatory drug (NSAID) naproxen (NAP). The two drugs were encapsulated in MIL-53(Al) individually to produce the DOX@MIL-53(Al) and NAP@MIL-53(Al) nanocarriers and also encapsulated together as a dual-drug formulation to produce the DOX* + NAP*@MIL-53(Al) nanocarrier. Also, the MOF nanoparticles were characterized using the SEM, XRD, FTIR, and DLS techniques. The SEM and XRD analysis proved the crystallinity of the MOF's structure, while the FTIR results revealed the successful encapsulation of drug molecules within the pores of the nanocarrier. In addition, the particle size distribution of MIL-53(Al) was determined from the DLS analysis, and the calculated average particle diameter was around 477 nm. Furthermore, the EE and EC of the nanocarriers were determined in the individual and combined drug scenarios. In the case of the DOX@MIL-53(Al), the average DOX EE and EC were around 92% and 16 wt.%, respectively, whereas, in the case of NAP@MIL-53(Al), the average NAP EE and EC were around 97.7% and 8.5 wt.%, respectively. On the other hand, in the DOX* + NAP*@MIL-53(Al) nanoparticles, the average DOX* EE and EC were 38.9% and 6.22 wt.%, respectively, while for NAP*, the average EE and EC were 70.2% and 4.49 wt.%, respectively. Furthermore, the *in vitro* release experiments demonstrated good pH and US dual-responsiveness, where the maximum US-triggered DOX and NAP release at a pH level of 7.4 was 53% and 95%, respectively. In comparison, it was around 90% and 36% at pH 5.3 for DOX and NAP, respectively. The nanocarrier displayed similar pH/US dual-responsive behavior in the dual-drug formulation, albeit exhibiting significantly slower release kinetics. Finally, the MTT results confirmed the low cytotoxicity of MIL-53(Al) at concentrations up to 1000 μg/ml, demonstrating their biocompatibility for use *in vivo* and future clinical trials.

Conflicts of Interest

There are no conflicts to declare.

Acknowledgments: This research was funded by the American University of Sharjah via the faculty research grants [grant numbers: FRG20-M-E84, FRG21-M-E63 and FRG20-L-E48]. The authors gratefully acknowledge the help of the Advanced Materials Research Lab at the University of Sharjah in conducting XRD and FTIR characterization tests.

REFERENCES

1. Siegel, R.L., Miller, K.D., Fuchs, H.E. and Jemal, A., **2022**. Cancer statistics, 2022. *CA: A Cancer Journal for Clinicians*, *72*(1), pp.7–33.
2. Nurgali, K., Jagoe, R.T. and Abalo, R., **2018**. Editorial: Adverse effects of cancer chemotherapy: Anything new to improve tolerance and reduce sequelae? *Frontiers in Pharmacology*, *9*.
3. Li, Y., Lu, A., Long, M., Cui, L., Chen, Z. and Zhu, L., **2019**. Nitroimidazole derivative incorporated liposomes for hypoxia-triggered drug delivery and enhanced therapeutic efficacy in patient-derived tumor xenografts. *Acta Biomaterialia*, *83*, pp.334–348.
4. Kanelli, M., Saleh, B., Webster, T.J., Vouyiouka, S. and Topakas, E., **2022**. Co-encapsulation of violacein and iron oxide in poly(lactic acid) nanoparticles for simultaneous antibacterial and anticancer applications. *Journal of Biomedical Nanotechnology*, *18*(3), pp.729–739.
5. Li, G., Xu, W., Shi, S., Chen, M. and Penget, D., **2022**. Construction of a new dual-responsive nano-drug delivery system for matrix metalloproteinases and adenosine triphosphate in ovarian cancer using nanomicelles. *Journal of Biomedical Nanotechnology*, *18*(3), pp.718–728.
6. Ibrahim, M., Sabouni, R. and Husseini, G., **2017**. Anti-cancer drug delivery using metal organic frameworks (MOFs). *Current Medicinal Chemistry*, *24*(2), pp.193–214.

7. Yang, J. and Yang, Y., **2020**. Metal–Organic frameworks for biomedical applications. *Small*, *16*(10), p.1906846.

8. Wang, L., Zheng, M. and Xie, Z., **2018**. Nanoscale metal–organic frameworks for drug delivery: A conventional platform with new promise. *Journal of Materials Chemistry B*, *6*(5), pp.707–717.

9. Liu, Y., Zhao, Y. and Chen, X., **2019**. Bioengineering of metal-organic frameworks for nanomedicine. *Theranostics*, *9*(11), pp.3122–3133.

10. Wang, Y., Yan, J., Wen, N., Xiong, H., Cai, S., He, Q., Hu, Y., Peng, D., Liu, Z. and Liu, Y., **2020**. Metal-organic frameworks for stimuli-responsive drug delivery. *Biomaterials*, *230*(June 2019), p.119619.

11. Carrillo-Carrión, C., **2020**. Nanoscale metal–organic frameworks as key players in the context of drug delivery: Evolution toward theranostic platforms. *Analytical and Bioanalytical Chemistry*, *412*(1), pp.37–54.

12. Xu, Z., Li, J., Li, X., Chen, Z., Chen, C., Ali Shah, S.A. and Wu, M., **2021**. An instantaneous metal organic framework to prepare ultra-high pore volume porous carbon for lithium ion capacitors. *Applied Surface Science*, *565*, p.150528.

13. Grünker, R., Bon, V., Müller, P., Stoeck, U., Krause, S., Mueller, U., Senkovska, I. and Kaskel, S., **2014**. A new metal–organic framework with ultra-high surface area. *Chemical Communications*, *50*(26), pp.3450–3452.

14. Li, P., Vermeulen, N.A., Malliakas, C.D., Gómez-Gualdrón, D.A., Howarth, A.J., Mehdi, B.L., Dohnalkova, A., Browning, N.D., O'Keeffe, M. and Farha, O.K., **2017**. Bottom-up construction of a superstructure in a porous uranium-organic crystal. *Science (New York, N.Y.)*, *356*(6338), pp.624–627.

15. Simon-Yarza, T., Mielcarek, A., Couvreur, P. and Serre, C., **2018**. Nanoparticles of metal-organic frameworks: On the road to in vivo efficacy in biomedicine. *Advanced Materials*, *30*(37), p.1707365.

16. Beg, S., Rahman, M., Jain, A., Saini, S., Midoux, P., Pichon, C., Ahmad, F.J. and Akhter, S., **2017**. Nanoporous metal organic frameworks as hybrid polymer–metal composites for drug delivery and biomedical applications. *Drug Discovery Today*, *22*(4), pp.625–637.

17. Zhou, Z., Vázquez-González, M. and Willner, I., **2021**. Stimuli-responsive metal–organic framework nanoparticles for controlled drug delivery and medical applications. *Chemical Society Reviews*, *50*(7), pp.4541–4563.

18. Cai, W., Wang, J., Chu, C., Chen, W., Wu, C. and Liu, G., **2019**. Metal–Organic framework-based stimuli-responsive systems for drug delivery. *Advanced Science*, *6*(1), p.1801526.

19. Jhaveri, A., Deshpande, P. and Torchilin, V., **2014**. Stimuli-sensitive nanopreparations for combination cancer therapy. *Journal of Controlled Release*, *190*, pp.352–370.

20. Karami, A., Mohamed, O., Ahmed, A., Husseini, G.A. and Sabouni, R., **2021**. Recent advances in metal-organic frameworks as anticancer drug delivery systems: A review. *Anticancer Agents in Medicinal Chemistry*, *21*(18), pp.2487–2504.

21. An, J., Hu, Y.-G., Li, C., Hou, X.-L., Cheng, K., Zhang, B., Zhang, R.-Y., Li, D.-Y., Liu, S.-J., Liu, B., Zhu, D. and Zhao, Y.-D., **2020**. A pH/Ultrasound dual-response biomimetic nanoplatform for nitric oxide gas-sonodynamic combined therapy and repeated ultrasound for relieving hypoxia. *Biomaterials*, *230*, p.119636.

22. Ahmed, A., Karami, A., Sabouni, R., Husseini, G.A. and Paul, V., **2021**. Ph and ultrasound dual-responsive drug delivery system based on PEG–folate-functionalized iron-based metal–organic framework for targeted doxorubicin delivery. *Colloids and Surfaces A: Physicochemical and Engineering Aspects*, *626*, p.127062.

23. Karami, A., Ahmed, A., Sabouni, R., Husseini, G.A., Sharabati, M.Al, AlSawaftah, N. and Paul, V., **2022**. Hybrid liposome/metal–organic framework as a promising dual-responsive nanocarriers for anticancer drug delivery. *Colloids and Surfaces B: Biointerfaces*, *217*, p.112599.

24. Husseini, G.A. and Pitt, W.G., **2008**. Micelles and nanoparticles for ultrasonic drug and gene delivery. *Advanced Drug Delivery Reviews*, *60*(10), pp.1137–1152.

25. Ibrahim, M., Sabouni, R., Husseini, G.A., Karami, A., Bai, R.G. and Mukhopadhyay, D., **2020**. Facile ultrasound-triggered release of calcein and doxorubicin from iron-based metal-organic frameworks. *Journal of Biomedical Nanotechnology*, *16*(9), pp.1359–1369.

26. Tanbour, R., Martins, M., G, A. Pitt, W., Husseini, A., G., **2016**. Drug delivery systems based on polymeric micelles and ultrasound: A review. *Current Pharmaceutical Design*, *22*(19), pp.2796–2807.

27. Awad, N.S., Paul, V., AlSawaftah, N.M., ter Haar, G., Allen, T.M., Pitt, W.G. and Husseini, G.A., **2021**. Ultrasound-responsive nanocarriers in cancer treatment: A review. *ACS Pharmacology & Translational Science*, *4*(2), pp.589–612.

28. Li, C., Xiong, Z., Zhang, J. and Wu, C., **2015**. The strengthening role of the amino group in metal–Organic framework MIL-53 (Al) for methylene blue and malachite green Dye adsorption. *Journal of Chemical & Engineering Data*, *60*(11), pp.3414–3422.

29. Xiao, Y., Han, T., Xiao, G., Ying, Y., Huang, H., Yang, Q., Liu, D. and Zhong, C., **2014**. Highly selective adsorption and separation of aniline/Phenol from aqueous solutions by microporous MIL-53(Al): A combined experimental and computational study. *Langmuir*, *30*(41), pp.12229–12235.

30. Li, Z., Wu, Y., Li, J., Zhang, Y., Zou, X. and Li, F., **2015**. The metal-organic framework MIL-53(Al) constructed from multiple metal sources: Alumina, aluminum hydroxide, and boehmite. *Chemistry-a European Journal*, *21*(18), pp.6913–6920.

31. Isiyaka, H.A., Jumbri, K., Sambudi, N.S., Zango, Z.U., Fathihah Abdullah, N.A., Saad, B. and Mustapha, A., **2020**. Adsorption of dicamba and MCPA onto MIL-53(Al) metal–organic framework: Response surface methodology and artificial neural network model studies. *Royal Society of Chemistry Advances*, *10*(70), pp.43213–43224.

32. Li, J., Wu, Y., Li, Z., Zhu, M. and Li, F., **2014**. Characteristics of arsenate removal from water by metal-organic frameworks (MOFs). *Water Science and Technology*, *70*(8), pp.1391–1397.

33. Khan, S., Guan, Q., Liu, Q., Qin, Z., Rasheed, B., Liang, X. and Yang, X., **2022**. Synthesis, modifications and applications of MILs metal-organic frameworks for environmental remediation: The cutting-edge review. *Science of the Total Environment*, *810*, p.152279.

34. Karami, A., Sabouni, R. and Ghommem, M., **2020**. Experimental investigation of competitive co-adsorption of naproxen and diclofenac from water by an aluminum-based metal-organic framework. *Journal of Molecular Liquids*, *305*, p.112808.

35. Al Sharabati, M. and Sabouni, R., **2020**. Selective removal of dual dyes from aqueous solutions using a metal organic framework (MIL-53(Al)). *Polyhedron*, *190*, p.114762.

36. Samokhvalov, A., **2018**. Aluminum metal–organic frameworks for sorption in solution: A review. *Coordination Chemistry Reviews*, *374*, pp.236–253.

37. Zhang, H., Jiang, W., Liu, R., Zhang, J., Zhang, D., Li, Z. and Luan, Y., **2017**. Rational design of metal organic framework nanocarrier-based codelivery system of doxorubicin hydrochloride/Verapamil hydrochloride for overcoming multidrug resistance with efficient targeted cancer therapy. *ACS Applied Materials & Interfaces*, *9*(23), pp.19687–19697.

38. Thorn, C.F., Oshiro, C., Marsh, S., Hernandez-Boussard, T., McLeod, H., Klein, T.E. and Altman, R.B., **2011**. Doxorubicin pathways: Pharmacodynamics and adverse effects. *Pharmacogenetics and Genomics*, *21*(7), pp.440–446.

39. Wongrakpanich, S., Wongrakpanich, A., Melhado, K. and Rangaswami, J., **2018**. A comprehensive review of non-steroidal anti-inflammatory drug Use in the elderly. *Aging and Disease*, *9*(1), pp.143–150.

40. Pereg, D. and Lishner M., **2005**. Non-steroidal anti-inflammatory drugs for the prevention and treatment of cancer. *Journal of Internal Medicine*, *258*(2), pp.115–123.

41. de Groot, D.J.A., de Vries, E.G.E., Groen, H.J.M. and de Jong, S., **2007**. Non-steroidal anti-inflammatory drugs to potentiate

chemotherapy effects: From lab to clinic. *Critical Reviews in Oncology/Hematology*, *61*(1), pp.52–69.

42. Ricchi, P., Zarrilli, R., di Palma, A. and Acquaviva, A.M., **2003**. Nonsteroidal anti-inflammatory drugs in colorectal cancer: From prevention to therapy. *British Journal of Cancer*, *88*(6), pp.803–807.

43. Sun, W. and Chen, G., **2016**. Impact and mechanism of non-steroidal anti-inflammatory drugs combined with chemotherapeutic drugs on human lung cancer-nude mouse transplanted tumors. *Oncology Letters*, *11*(6), pp.4193–4199.

44. Hiľovská, L., Jendželovský, R. and Fedoročko, P., **2015**. Potency of non-steroidal anti-inflammatory drugs in chemotherapy. *Molecular and Clinical Oncology*, *3*(1), pp.3–12.

45. Yu, C., Li, W., Liu, J., Lu, J. and Feng, J., **2018**. Autophagy: Novel applications of nonsteroidal anti-inflammatory drugs for primary cancer. *Cancer Medicine*, *7*(2), pp.471–484.

46. Read, N.W. and Sugden, K., **1988**. Gastrointestinal dynamics and pharmacology for the optimum design of controlled-release oral dosage forms. *Critical Reviews in Therapeutic Drug Carrier Systems*, *4*(3), pp.221–263.

47. Adhikari, C., Das, A. and Chakraborty, A., **2015**. Zeolitic imidazole framework (ZIF) nanospheres for easy encapsulation and controlled release of an anticancer drug doxorubicin under different external stimuli: A Way toward smart drug delivery system. *Molecular Pharmaceutics*, *12*(9), pp.3158–3166.

48. Abid, H.R., Rada, Z.H., Shang, J. and Wang, S., **2016**. Synthesis, characterization, and CO_2 adsorption of three metal-organic frameworks (MOFs): MIL-53, MIL-96, and amino-MIL-53. *Polyhedron*, *120*, pp.103–111.

49. Nowroozi-Nejad, Z., Bahramian, B. and Hosseinkhani, S., **2019**. A fast and efficient stabilization of firefly luciferase on MIL-53(Al) via surface adsorption mechanism. *Research on Chemical Intermediates*, *45*(4), pp.2489–2501.

50. Loiseau, T., Serre, C., Huguenard, C., Fink, G., Taulelle, F., Henry, M., Bataille, T. and Férey, G., **2004**. A rationale for the large breathing of the porous aluminum terephthalate (MIL-53) upon hydration. *Chemistry—A European Journal*, *10*(6), pp.1373–1382.

51. Liu, J.-F., Mu, J.-C., Qin, R.-X. and Ji, S.-F., **2019**. Pd nanoparticles immobilized on MIL-53(Al) as highly effective bifunctional catalysts for oxidation of liquid methanol to methyl formate. *Petroleum Science*, *16*(4), pp.901–911.

52. Meilikhov, M., Yusenko, K. and Fischer, R.A., **2009**. The adsorbate structure of ferrocene inside [Al(OH)(bdc)] x (MIL-53): A powder X-ray diffraction study. *Dalton Trans*, (4), pp.600–602.

53. Farboudi, A., Mahboobnia, K., Chogan, F., Karimi, M., Askari, A., Banihashem, S., Davaran, S. and Irani, M., **2020**. Uio-66 metal organic framework nanoparticles loaded carboxymethyl chitosan/poly ethylene oxide/polyurethane core-shell nanofibers for controlled release of doxorubicin and folic acid. *International Journal of Biological Macromolecules*, *150*.

54. Gao, Y., Liu, K., Kang, R., Xia, J., Yu, G. and Deng, S., **2018**. A comparative study of rigid and flexible MOFs for the adsorption of pharmaceuticals: Kinetics, isotherms and mechanisms. *Journal of Hazardous Materials*, *359*(March), pp.248–257.

55. Ahadi, N., Askari, S., Fouladitajar, A. and Akbari, I., **2022**. Facile synthesis of hierarchically structured MIL-53(Al) with superior properties using an environmentally-friendly ultrasonic method for separating lead ions from aqueous solutions. *Scientific Reports 2022*, *12*(1), pp.1–17.

56. Zhang, L., Gao, Y., Sun, S., Li, Z., Wu, A. and Zeng, L., **2020**. Ph-responsive metal–organic framework encapsulated gold nanoclusters with modulated release to enhance photodynamic therapy/chemotherapy in breast cancer. *Journal of Materials Chemistry B*, *8*(8), pp.1739–1747.

57. Hobbs, S.K., Monsky, W.L., Yuan, F., Roberts, W.G., Griffith, L., Torchilin, V.P. and Jain, R.K., **1998**. Regulation of transport pathways in tumor vessels: Role of tumor type and microenvironment. *Proceedings of the National Academy of Sciences*, *5*(8), pp.4607–4612.

58. Jiang, J.X., Keating, J.J., Jesus, E.M.D., Judy, R.P., Madajewski, B., Venegas, O., Okusanya, O.T. and Singhal, S., **2015**. Optimization of the enhanced permeability and retention effect for near-infrared imaging of solid tumors with indocyanine green. *American Journal of Nuclear Medicine and Molecular Imaging*, *5*(4), pp.390–400.

59. Gupta, S.A., **2016**. Role of particle size, shape, and stiffness in design of intravascular drug delivery systems: Insights from computations, experiments, and nature. *Wiley Interdisciplinary Reviews: Nanomedicine and Nanobiotechnology*, *8*(2), pp.255–270.

60. Gaumet, M., Vargas, A., Gurny, R. and Delie, F., **2008**. Nanoparticles for drug delivery: The need for precision in reporting particle size parameters. *European Journal of Pharmaceutics and Biopharmaceutics*, *69*(1), pp.1–9.

61. Danaei, M., Dehghankhold, M., Ataei, S., Hasanzadeh Davarani, F., Javanmard, R., Dokhani, A., Khorasani, S. and Mozafari, M., **2018**. Impact of particle size and polydispersity index on the clinical applications of lipidic nanocarrier systems. *Pharmaceutics*, *10*(2), p.57.

62. Bertrand, N., Wu, J., Xu, X., Kamaly, N. and Farokhzad, O.C., **2014**. Cancer nanotechnology: The impact of passive and active targeting in the era of modern cancer biology. *Advanced Drug Delivery Reviews*, *66*, pp.2–25.

63. Huang, D., Liu, Y., Liu, Y., Di, D., Wang, H. and Yang, W., **2019**. Preparation of metal–organic frameworks with bimetallic linkers and corresponding properties. *New Journal of Chemistry*, *43*(19), pp.7243–7250.

64. Chen, X.Y., Hoang, V.T., Rodrigue, D. and Kaliaguine, S., **2013**. Optimization of continuous phase in amino-functionalized metal-organic framework (MIL-53) based co-polyimide mixed matrix membranes for CO_2/CH_4 separation. *RSC Advances*, *3*(46), pp.24266–24279.

65. Yang, C.-X., Ren, H.-B. and Yan, X.-P., **2013**. Fluorescent metal–Organic framework MIL-53(Al) for highly selective and sensitive detection of Fe^{3+} in aqueous solution. *Analytical Chemistry*, *85*(15), pp.7441–7446.

66. Horcajada, P., Gref, R., Baati, T., Allan, P.K., Maurin, G., Couvreur, P., Férey, G., Morris, R.E. and Serre, C., **2012**. Metal–Organic frameworks in biomedicine. *Chemical Reviews*, *112*(2), pp.1232–1268.

67. Li, X., Porcino, M., Qiu, J., Constantin, D., Martineau-Corcos, C. and Gref, R., **2021**. Doxorubicin-loaded metal-organic frameworks nanoparticles with engineered cyclodextrin coatings: Insights on drug location by solid state NMR spectroscopy. *Nanomaterials*, *11*(4), p.945.

68. Feng, Y., Wang, C., Ke, F., Zang, J. and Zhu, J., **2018**. MIL-100(Al) gels as an excellent platform loaded with doxorubicin hydrochloride for pH-triggered drug release and anticancer effect. *Nanomaterials*, *8*(6), p.446.

69. Lin, S., Zhao, Y. and Yun, Y.-S.S., **2018**. Highly effective removal of nonsteroidal anti-inflammatory pharmaceuticals from water by Zr(IV)-Based metal–Organic framework: Adsorption performance and mechanisms. *ACS Applied Materials & Interfaces*, *10*(33), pp.28076–28085.